Hindawi Publishing Corporation
EURASIP Journal on Wireless Communications and Networking
Volume 2010, Article ID 385872, 9 pages
doi:10.1155/2010/385872

Research Article

Distributed Space-Time Block Code over Mixed Rayleigh and Rician Frequency-Selective Fading Channels

Quoc-Tuan Vien,[1,2] Le-Nam Tran,[1] and Een-Kee Hong[1]

[1] *School of Electronics and Information, Kyung Hee University, Yongin, Geonggi 446-701, Republic of Korea*
[2] *School of Engineering and Computing, Glasgow Caledonian University, Cowcaddens Road, Glasgow G4 0BA, UK*

Correspondence should be addressed to Een-Kee Hong, ekhong@khu.ac.kr

Received 28 October 2009; Revised 18 March 2010; Accepted 9 June 2010

Academic Editor: Mohamed Hossam Ahmed

This paper proposes a new distributed space-time block code (DSTBC) over frequency-selective fading channels for two-hop amplify and forward relay networks, consisting of a source node ($\mathcal{S}$), two relay nodes ($\mathcal{R}_1$ and $\mathcal{R}_2$), and a destination node ($\mathcal{D}$). The proposed DSTBC is designed to achieve maximal spatial diversity gain and decoupling detection of data blocks with a low-complexity receiver. To achieve these two goals, $\mathcal{S}$ uses zero-sequence padding, and relay nodes precode the received signals with a proper precoding matrix. The pairwise error probability (PEP) analysis is provided to investigate the achievable diversity gain of the proposed DSTBC for a general channel model in which one hop is modeled by Rayleigh fading and the other by Rician fading. This mixed Rayleigh-Rician channel model allows us to analyze two typical scenarios where $\{\mathcal{R}_i\}$ are in the neighborhood of either $\mathcal{S}$ or $\mathcal{D}$.

1. Introduction

The reliability of wireless communications over fading channels can be greatly improved by the use of diversity schemes. For multiple-input multiple-output (MIMO) systems, transmitted diversity can be realized in the form of space-time block codes (STBCs) [1, 2]. With low-complexity maximum-likelihood (ML) decodability and high achievable diversity gain, STBCs are widely used for wireless communications. Generally, the conventional STBCs were designed for the colocated antennas, and thus are easily deployed at the base station to improve the performance of the downlink transmission. Nevertheless, the realization of STBCs is impractical in the uplink transmission due to the constraints on size and hardware complexity in mobile handsets. Fortunately, mobile users can cooperate to form a virtual multiple-antenna system, which is now known as cooperative diversity [3, 4].

The distributed space-time block codes can be viewed as the distributed implementation of conventional STBCs for cooperative communications. Originally, the DSTBCs were proposed for flat-fading channels [5–7]. The problem of DSTBC in frequency-selective fading channels was investigated in [8] with decode-and-forward (DF) relaying, and in [9] with amplify-and-forward (AF) relaying. However, these DSTBCs were devised for relay networks where there exists one active relay node and a direct communication link between the source and the final destination.

In this paper, we design a new DSTBC for two-hop relay networks [6, 7] over frequency-selective fading channels with AF protocol, where there are two active relay nodes. The proposed DSTBC operates as follows: in the first time slot, the source ($\mathcal{S}$) sends two blocks of information data to two relays ($\mathcal{R}_1$ and $\mathcal{R}_2$). What is remarkable in our proposed DSTBC is that one of the two relays precodes its received signals that will be sent to the destination ($\mathcal{D}$) in the next time slot. The precoding matrix is designed such that each relay conveys a distinct column of the block Alamouti scheme (see, e.g., [1, 10, 11]). Our main contributions in this paper are summarized in brief as follows.

(i) With our proposed DSTBC, the data rate of 1/2 is achieved, which is proved to be the maximum data rate for two-hop relaying networks. As we can see later, the extension of [9] to two relays results in a rate of 1/3.

(ii) We propose the precoding matrix at the relays such that the decoupling detection of two data blocks in both time and frequency domains is possible at $\mathcal{D}$. The PEP analysis is carried out with ML detection in time domain, and numerical results are obtained with minimum mean square error (MMSE) receiver in frequency domain.

(iii) We study the achievable diversity gain of the proposed DSTBC for the general scenario where the relays are located near the source or the destination, that is, one of the two hops ($\mathcal{S}$ to $\{\mathcal{R}_i\}$ or $\{\mathcal{R}_i\}$ to $\mathcal{D}$) is line-of-sight (LOS) transmission, while the other is nonline-of-sight (NLOS) transmission. Accordingly, the considered channel model is a mix of Rayleigh and Rician fading.

The theoretical results prove that our proposed scheme achieves the spatial diversity order of $\min(L_{SR_1}, L_{R_1D}) + \min(L_{SR_2}, L_{R_2D}) + 2$, where L_{SR_j} and L_{R_jD} are the channel memory lengths for the links from $\mathcal{S}$ to $\mathcal{R}_j$ and from $\mathcal{R}_j$ to $\mathcal{D}$, respectively. The analysis also shows that the n-factor of Rician fading in the LOS component provides a coding gain to the PEP performance. It means that as the n-factor increases, a better performance is observed.

The rest of this paper is organized as follows In Section 2, we describe the system model of the proposed DSTBC and the proof of decoupling capability in time domain and frequency domain. Performance analysis is presented in Section 3. We present the numerical results in Section 4, and Section 5 concludes this paper.

Notation. Bold lower and upper case letters represent vectors and matrices, respectively; $(\cdot)^T$, $(\cdot)^*$, and $(\cdot)^{\mathcal{H}}$ denote transpose, complex conjugate, and Hermitian transpose operations, respectively; $\mathbf{I}_M$ and 0_M denote an identity matrix and an all-zero matrix of size $M \times M$; $E[\cdot]$ denotes the expectation; $\|\cdot\|$ denotes the Euclidean norm of a vector; $\mathbf{F}_M$ stands for a Fast Fourier Transform (FFT) matrix of size $M \times M$; $\mathcal{S} \to \mathcal{R}_i$ and $\mathcal{R}_i \to \mathcal{D}$ represent the links from the source ($\mathcal{S}$) to the ith relay ($\mathcal{R}_i$) and from $\mathcal{R}_i$ to the destination ($\mathcal{D}$), respectively.

2. System Model and the Proposed DSTBC

We consider a four-node wireless relay network shown in Figure 1, where the source terminal cannot communicate directly with the intended destination. The data transmission from $\mathcal{S}$ to $\mathcal{D}$ is completed via two-hop protocol [6, 7] with the assistance of two relays $\mathcal{R}_1$ and $\mathcal{R}_2$. The frequency-selective channel from $\mathcal{X}$ to $\mathcal{Y}$ is characterized by $\mathbf{h}_{XY} = [h_{XY}(0), \ldots, h_{XY}(L_{XY})]^T$, where L_{XY} is the channel memory order. Two transmitted data blocks $\mathbf{x}_1$ and $\mathbf{x}_2$ of length M, shown in Figure 1, are created by padding a zero sequence of length L to two information data blocks $\mathbf{s}_i$, $i = 1, 2$, of length B. To achieve the decoupling property of data detection, the length of the zero sequence must satisfy $L \geq \max(L_{SR_1} + L_{R_1D}, L_{SR_2} + L_{R_2D})$ [9]. This condition makes circulant channel matrices from source to relays and relays to destination.

In the first time slot, the source serially transmits two data blocks to two relays. In the next time slot, one relay only amplifies and forwards its received signals, while the other precodes its received data blocks by a precoding matrix before transmitting to the destination as illustrated in Figure 1. The idea behind our design is that precoding in $\mathcal{R}_2$ is designed to send the second column of the block Alamouti's scheme (see, e.g., [1, 11]) to $\mathcal{D}$. This enables the decoupling detection of two data blocks at the destination and achieves a rate of 1/2. To achieve the same goal in the considered scenario, the source with repetition code in [9], which is devised for one-relay system, must send two columns during two time slots. Thus, the rate of this scheme is reduced to 1/3. Recall that the maximum achievable data rate of an N-relay repetition-coding network is $1/(N+1)$ [12]. Clearly, our design can achieve a higher data rate transmission.

We now proceed to prove that our proposed DSTBC can decouple the detection of two data blocks. Throughout this paper, the superscript j denotes the relay index, while the subscript i refers to data block index. The received signal at the relay is given by

$$\mathbf{r}_i^j = \sqrt{E_{SR_j}}\mathbf{H}_{SR_j}\mathbf{x}_i + \boldsymbol{\eta}_i^j, \quad i = 1, 2, \ j = 1, 2, \tag{1}$$

where E_{SR_j} is the average energy of $\mathcal{S} \to \mathcal{R}_j$ link; $\mathbf{H}_{SR_j}$ is the $M \times M$ circulant channel matrix of $\mathcal{S} \to \mathcal{R}_j$ link; $\boldsymbol{\eta}_i^j$ is the white Gaussian noise vector at the jth relay with each entry having zeromean and variance of $N_0/2$ per dimension. For any $M \times M$ circulant matrix $\mathbf{H}_{XY}$, its (k, l) entry is written as $[\mathbf{H}_{XY}]_{k,l} = \mathbf{h}_{XY}((k-l) \bmod M)$.

At $\mathcal{R}_2$, the received data $[(\mathbf{r}_1^2)^T, (\mathbf{r}_2^2)^T]^T$ is conjugated, followed by the precoding operation which is denoted by precoding matrix $\mathbf{P}$

$$\mathbf{P} = \begin{bmatrix} 0_M & -\mathbf{P}_M^K \\ \mathbf{P}_M^K & 0_M \end{bmatrix}, \tag{2}$$

where the matrix $\mathbf{P}_M^K$ is designed as

$$\mathbf{P}_M^K = \begin{bmatrix} \mathbf{P}_1 & 0_{K\times(M-K)} \\ 0_{(M-K)\times K} & \mathbf{P}_2 \end{bmatrix}. \tag{3}$$

In (3), the matrix $\mathbf{P}_1$ of size $K \times K$ and the matrix $\mathbf{P}_2$ of size $(M-K) \times (M-K)$ have (l, k) element given, respectively, by

$$\begin{aligned} \mathbf{P}_1(l,k) &= \begin{cases} 1, & \text{if } k = K - l + 1, \\ 0, & \text{otherwise,} \end{cases} \\ \mathbf{P}_2(l,k) &= \begin{cases} 1, & \text{if } k = M - K - l + 1, \\ 0, & \text{otherwise.} \end{cases} \end{aligned} \tag{4}$$

We choose $K = B + L_{SR_2}$ to ensure that, after precoding, at least last L_{SR_2} samples of $-\mathbf{P}_M^K\mathbf{r}_2^2$ and $\mathbf{P}_M^K\mathbf{r}_1^2$ are all zeros to make the circulant channel matrix $\mathcal{R}_2 \to \mathcal{D}$. Before transmitting the signals to the destination, the relay $\mathcal{R}_j$

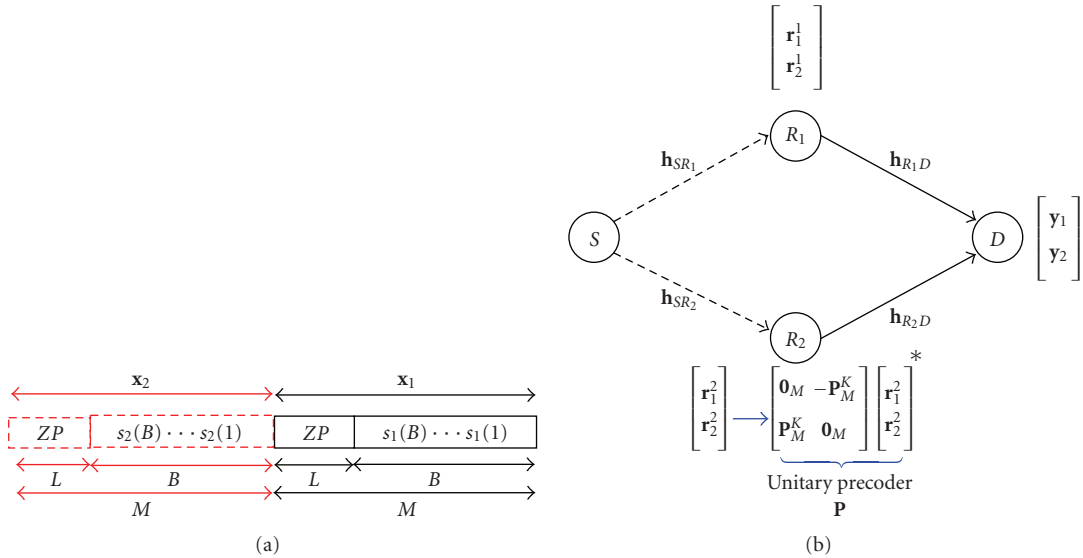

FIGURE 1: System model and data structures.

normalizes its signals by $(E_{SR_j} + N_0)$ to have unit average energy. The received signals at the destination are written by

$$\begin{aligned}\mathbf{y}_1 &= \sqrt{E_{R_1D}}\mathbf{H}_{R_1D}\tilde{\mathbf{r}}_1^1 - \sqrt{E_{R_2D}}\mathbf{H}_{R_2D}\mathbf{P}_M^K\left(\tilde{\mathbf{r}}_2^2\right)^* \\ &\quad + \boldsymbol{\eta}_{D,1}, \\ \mathbf{y}_2 &= \sqrt{E_{R_1D}}\mathbf{H}_{R_1D}\tilde{\mathbf{r}}_2^1 + \sqrt{E_{R_2D}}\mathbf{H}_{R_2D}\mathbf{P}_M^K\left(\tilde{\mathbf{r}}_1^2\right)^* \\ &\quad + \boldsymbol{\eta}_{D,2},\end{aligned} \tag{5}$$

where E_{R_jD} is the average energy of $\mathcal{R}_j \rightarrow \mathcal{D}$ link; $\tilde{\mathbf{r}}_i^j$ is the normalized received signal; $\mathbf{H}_{R_jD}$ is the $M \times M$ circulant matrix, denoting the channel $\mathcal{R}_j \rightarrow \mathcal{D}$; $\boldsymbol{\eta}_{D,i}$ is white Gaussian noise vector at the destination with each entry having zeromean and variance of $N_0/2$.

Using (1), we can rewrite (5) as

$$\begin{aligned}\mathbf{y}_1 &= \sqrt{\frac{E_{R_1D}E_{SR_1}}{E_{SR_1}+N_0}}\mathbf{H}_{R_1D}\mathbf{H}_{SR_1}\mathbf{x}_1 - \sqrt{\frac{E_{R_2D}E_{SR_2}}{E_{SR_2}+N_0}}\mathbf{H}_{R_2D}\mathbf{P}_M^K\mathbf{H}_{SR_2}^*\mathbf{x}_2^* \\ &\quad + \boldsymbol{\eta}_1, \\ \mathbf{y}_2 &= \sqrt{\frac{E_{R_1D}E_{SR_1}}{E_{SR_1}+N_0}}\mathbf{H}_{R_1D}\mathbf{H}_{SR_1}\mathbf{x}_2 + \sqrt{\frac{E_{R_2D}E_{SR_2}}{E_{SR_2}+N_0}}\mathbf{H}_{R_2D}\mathbf{P}_M^K\mathbf{H}_{SR_2}^*\mathbf{x}_1^* \\ &\quad + \boldsymbol{\eta}_2,\end{aligned} \tag{6}$$

where $\boldsymbol{\eta}_1$ and $\boldsymbol{\eta}_2$ include the Gaussian noise of relays and destination. It is common to normalize the noise variance in (6) to be $N_0/2$, which results in

$$\mathbf{y}_1' = \alpha_1\mathbf{H}_{R_1D}\mathbf{H}_{SR_1}\mathbf{x}_1 - \alpha_2\mathbf{H}_{R_2D}\mathbf{P}_M^K\mathbf{H}_{SR_2}^*\mathbf{x}_2^* + \boldsymbol{\eta}_1', \tag{7}$$

$$\mathbf{y}_2' = \alpha_1\mathbf{H}_{R_1D}\mathbf{H}_{SR_1}\mathbf{x}_2 + \alpha_2\mathbf{H}_{R_2D}\mathbf{P}_M^K\mathbf{H}_{SR_2}^*\mathbf{x}_1^* + \boldsymbol{\eta}_2'. \tag{8}$$

The values of normalization factors in (7) and (8) are defined by

$$\alpha_i = \left[\frac{\beta_{j\neq i}\gamma_i E_{SR_i}}{\beta_1\beta_2 + \beta_2\gamma_1\sum_{l=0}^{L_{R_1D}}\left|\mathbf{h}_{R_1D}(l)\right|^2 + \beta_1\gamma_2\sum_{l=0}^{L_{R_2D}}\left|\mathbf{h}_{R_2D}(l)\right|^2}\right]^{1/2}, \tag{9}$$

where $\beta_i = 1 + E_{SR_i}/N_0$ and $\gamma_i = E_{R_iD}/N_0$ for $i, j \in \{1, 2\}$.

By conjugating, and multiplying both sides of (8) with $\mathbf{P}_M^K$, and noting that $\mathbf{P}_M^K\mathbf{H}^*\mathbf{P}_M^K = \mathbf{H}^{\mathcal{H}}$ for any circulant matrix $\mathbf{H}$, we can rewrite (8) as

$$\mathbf{y}_2'' = \alpha_2\mathbf{H}_{R_2D}^{\mathcal{H}}\mathbf{H}_{SR_2}\mathbf{x}_1 + \alpha_1\mathbf{H}_{R_1D}^{\mathcal{H}}\mathbf{H}_{SR_1}^{\mathcal{H}}\mathbf{P}_M^K\mathbf{x}_2^* + \boldsymbol{\eta}_2''. \tag{10}$$

For mathematical convenience, we group (7) and (10) in vector-matrix form as

$$\begin{bmatrix}\mathbf{y}_1' \\ \mathbf{y}_2''\end{bmatrix} = \mathbf{H}\begin{bmatrix}\mathbf{x}_1 \\ \mathbf{P}_M^K\mathbf{x}_2^*\end{bmatrix} + \begin{bmatrix}\boldsymbol{\eta}_1' \\ \boldsymbol{\eta}_2''\end{bmatrix}, \tag{11}$$

where

$$\mathbf{H} \triangleq \begin{bmatrix}\alpha_1\mathbf{H}_{R_1D}\mathbf{H}_{SR_1} & -\alpha_2\mathbf{H}_{R_2D}\mathbf{H}_{SR_2}^{\mathcal{H}} \\ \alpha_2\mathbf{H}_{R_2D}^{\mathcal{H}}\mathbf{H}_{SR_2} & \alpha_1\mathbf{H}_{R_1D}^{\mathcal{H}}\mathbf{H}_{SR_1}^{\mathcal{H}}\end{bmatrix}. \tag{12}$$

Let us denote $\boldsymbol{\Omega} = [\alpha_1^2\langle\mathbf{H}_{SR_1}\rangle^2\langle\mathbf{H}_{R_1D}\rangle^2 + \alpha_2^2\langle\mathbf{H}_{SR_2}\rangle^2\langle\mathbf{H}_{R_2D}\rangle^2]^{1/2}$, where $\langle\mathbf{H}_{XY}\rangle^2 \triangleq \mathbf{H}_{XY}\mathbf{H}_{XY}^{\mathcal{H}} = \mathbf{H}_{XY}^{\mathcal{H}}\mathbf{H}_{XY}$ for any circulant matrix $\mathbf{H}_{XY}$. Then, $\mathbf{H}^{\mathcal{H}}\mathbf{H} = \mathbf{I}_2 \otimes \boldsymbol{\Omega}^2$ is a block-diagonal matrix. By multiplying both sides of (11) with the unitary matrix $(\mathbf{I}_2 \otimes \boldsymbol{\Omega}^{-1})\mathbf{H}^{\mathcal{H}}$, we can decouple the detection of two data blocks. That means two data blocks can be detected independently, rather than joint

detection, without any loss of gain, which is based on the following model

$$\begin{bmatrix}\mathbf{z}_1\\ \mathbf{z}_2\end{bmatrix} = \left(\mathbf{I}_2 \otimes \mathbf{\Omega}^{-1}\right)\mathbf{H}^{\mathcal{H}}\begin{bmatrix}\mathbf{y}_1'\\ \mathbf{y}_2''\end{bmatrix} = \begin{bmatrix}\mathbf{\Omega}\mathbf{x}_1\\ \mathbf{\Omega}\mathbf{P}_M^K\mathbf{x}_2^*\end{bmatrix} + \begin{bmatrix}\overline{\boldsymbol{\eta}}_1\\ \overline{\boldsymbol{\eta}}_2\end{bmatrix}, \tag{13}$$

where $\overline{\boldsymbol{\eta}}_i$ is the Gaussian noise vector resulting from the space-time decoupling.

Since the general ML detection or standard equalization techniques based on (13) require complex receiver, we introduce the decoupling in the frequency domain that allows for low-complexity equalizers [13].

We notice that any $M \times M$ circulant matrix $\mathbf{H}$ can be diagonalized as $\mathbf{H} = \mathbf{F}_M^{\mathcal{H}}\mathbf{\Lambda}\mathbf{F}_M$, where $\mathbf{\Lambda}$ is the $M \times M$ diagonal matrix whose diagonal elements are the DFT of the first column of $\mathbf{H}$. Taking the DFT of both sides of (11) results in

$$\begin{bmatrix}\widetilde{\mathbf{y}}_1\\ \widetilde{\mathbf{y}}_2\end{bmatrix} = \begin{bmatrix}\mathbf{F}_M\mathbf{y}_1'\\ \mathbf{F}_M\mathbf{y}_2''\end{bmatrix} = \mathbf{\Lambda}\begin{bmatrix}\widetilde{\mathbf{x}}_1\\ \widetilde{\mathbf{x}}_2\end{bmatrix} + \begin{bmatrix}\widetilde{\boldsymbol{\eta}}_1\\ \widetilde{\boldsymbol{\eta}}_2\end{bmatrix}, \tag{14}$$

where $\widetilde{\mathbf{x}}_1 = \mathbf{F}_M\mathbf{x}_1$, $\widetilde{\mathbf{x}}_2 = \mathbf{F}_M\mathbf{P}_M^K\mathbf{x}_2^*$,

$$\mathbf{\Lambda} = \begin{bmatrix}\alpha_1\mathbf{\Lambda}_{R_1D}\mathbf{\Lambda}_{SR_1} & -\alpha_2\mathbf{\Lambda}_{R_2D}\mathbf{\Lambda}_{SR_2}^*\\ \alpha_2\mathbf{\Lambda}_{R_2D}^*\mathbf{\Lambda}_{SR_2} & \alpha_1\mathbf{\Lambda}_{R_1D}^*\mathbf{\Lambda}_{SR_1}^*\end{bmatrix}. \tag{15}$$

Let us denote $\mathbf{\Psi} = [\alpha_1^2\langle\mathbf{\Lambda}_{SR_1}\rangle^2\langle\mathbf{\Lambda}_{R_1D}\rangle^2 + \alpha_2^2\langle\mathbf{\Lambda}_{SR_2}\rangle^2\langle\mathbf{\Lambda}_{R_2D}\rangle^2]^{1/2}$. Then, $\mathbf{\Lambda}^{\mathcal{H}}\mathbf{\Lambda} = \mathbf{I}_2 \otimes \mathbf{\Psi}^2$ is a block-diagonal matrix. By multiplying both sides of (14) with the unitary matrix $(\mathbf{I}_2 \otimes \mathbf{\Psi}^{-1})\mathbf{\Lambda}^{\mathcal{H}}$, we can decouple the detection of each data block in frequency domain as

$$\widetilde{\mathbf{z}}_i = \mathbf{\Psi}\widetilde{\mathbf{x}}_i + \boldsymbol{\omega}_i, \quad i = 1, 2. \tag{16}$$

Since the matrix $\mathbf{\Psi}$ is diagonal, (16) can be decomposed into a set of M scalar equations

$$\widetilde{z}_k = \Psi_k\widetilde{x}_k + \omega_k, \quad k = 0, 1, \ldots, M-1. \tag{17}$$

In (17), we omit the dependency of subscript i because the detection of two data blocks is based on the same model. Typical frequency domain equalizers in [13] can be applied to the outputs of decoupling process.

3. Performance Analysis

In this section, we derive the PEP expression of the proposed DSTBC model over frequency-selective fading channels based on the joint channel model (11), where the links $\mathcal{S} \to \mathcal{R}$ and $\mathcal{R} \to \mathcal{D}$ experience Rician fading and Rayleigh fading, respectively. For the case when $\mathcal{S} \to \mathcal{R}$ and $\mathcal{R} \to \mathcal{D}$ are Rayleigh fading and Rician fading, the PEP expression can be similarly obtained with some interchanged parameters.

Defining the decoded codeword vector as $\hat{\mathbf{x}}$ and the Euclidean distance between $\mathbf{x}$ and $\hat{\mathbf{x}}$ as $d(\mathbf{x}, \hat{\mathbf{x}})$, the conditional PEP under fading channels is given by

$$P(\mathbf{x} \longrightarrow \hat{\mathbf{x}} \mid \mathbf{h}_{SR_1}, \mathbf{h}_{SR_2}, \mathbf{h}_{R_1D}, \mathbf{h}_{R_2D}) = Q\left(\sqrt{\frac{d^2(\mathbf{x}, \hat{\mathbf{x}})}{2N_0}}\right), \tag{18}$$

where $Q(\cdot)$ is the Q function. By applying Chernoff bound to Q function, this PEP is upper bounded by

$$P(\mathbf{x} \longrightarrow \hat{\mathbf{x}} \mid \mathbf{h}_{SR_1}, \mathbf{h}_{SR_2}, \mathbf{h}_{R_1D}, \mathbf{h}_{R_2D}) \le \exp\left(-\frac{d^2(\mathbf{x}, \hat{\mathbf{x}})}{4N_0}\right). \tag{19}$$

The Euclidean distance in (19) is calculated by

$$\begin{aligned} d^2(\mathbf{x}, \hat{\mathbf{x}}) = {} & \alpha_1^2\left|\left|\mathbf{H}_{R_1D}\mathbf{H}_{SR_1}(\mathbf{x}_1 - \hat{\mathbf{x}}_1)\right|\right|^2 \\ & + \alpha_2^2\left|\left|\mathbf{H}_{R_2D}\mathbf{H}_{SR_2}\mathbf{P}_M^K(\mathbf{x}_2 - \hat{\mathbf{x}}_2)\right|\right|^2. \end{aligned} \tag{20}$$

Using the fact in [9], we can approximate (20) to

$$\begin{aligned} d^2(\mathbf{x}, \hat{\mathbf{x}}) &\approx \frac{\alpha_1^2}{M}\left|\left|\mathbf{H}_{R_1D}\right|\right|^2\left|\left|\mathbf{H}_{SR_1}\mathbf{e}_1\right|\right|^2 + \frac{\alpha_2^2}{M}\left|\left|\mathbf{H}_{R_2D}\right|\right|^2\left|\left|\mathbf{H}_{SR_2}\mathbf{e}_2\right|\right|^2 \\ &\approx \frac{\alpha_1^2}{M}\left|\left|\mathbf{H}_{SR_1}\right|\right|^2\left|\left|\mathbf{H}_{R_1D}\mathbf{e}_1\right|\right|^2 + \frac{\alpha_2^2}{M}\left|\left|\mathbf{H}_{R_2D}\right|\right|^2\left|\left|\mathbf{H}_{SR_2}\mathbf{e}_2\right|\right|^2 \\ &\approx \frac{\alpha_1^2}{M}\left|\left|\mathbf{H}_{R_1D}\right|\right|^2\left|\left|\mathbf{H}_{SR_1}\mathbf{e}_1\right|\right|^2 + \frac{\alpha_2^2}{M}\left|\left|\mathbf{H}_{SR_2}\right|\right|^2\left|\left|\mathbf{H}_{R_2D}\mathbf{e}_2\right|\right|^2 \\ &\approx \frac{\alpha_1^2}{M}\left|\left|\mathbf{H}_{SR_1}\right|\right|^2\left|\left|\mathbf{H}_{R_1D}\mathbf{e}_1\right|\right|^2 + \frac{\alpha_2^2}{M}\left|\left|\mathbf{H}_{SR_2}\right|\right|^2\left|\left|\mathbf{H}_{R_2D}\mathbf{e}_2\right|\right|^2, \end{aligned} \tag{21}$$

where $\mathbf{e}_i = (\mathbf{x}_i - \hat{\mathbf{x}}_i)$, and $i = 1, 2$. We note that $\|\mathbf{H}_{XY}\|^2 = M\sum_{l_{XY}=0}^{L_{XY}}|\mathbf{h}_{XY}(l_{XY})|^2$, and $\|\mathbf{H}_{XY}\mathbf{e}_i\|^2 = \sum_{l_{XY}=0}^{L_{XY}}\boldsymbol{\lambda}_i(l_{XY})|\boldsymbol{\nu}_i(l_{XY})|^2$; $i = 1, 2$. $\boldsymbol{\lambda}_i(l_{XY})$ denotes the eigenvalue of codeword difference matrix, and $\boldsymbol{\nu}$ is zero-mean complex Gaussian vectors with unit variance. In (21), we mean that the distance can be approximated by one of four possible forms. Each component of the summations of the right hand side of (21) can be expressed by one of the two following factors

$$d_1^2 = \sum_{l_{RD}=0}^{L_{RD}}|\mathbf{h}_{RD}(l_{RD})|^2\sum_{l_{SR}=0}^{L_{SR}}\boldsymbol{\lambda}(l_{SR})|\boldsymbol{\nu}(l_{SR})|^2, \tag{22}$$

or

$$d_2^2 = \sum_{l_{SR}=0}^{L_{SR}}|\mathbf{h}_{SR}(l_{SR})|^2\sum_{l_{RD}=0}^{L_{RD}}\boldsymbol{\lambda}(l_{RD})|\boldsymbol{\nu}(l_{RD})|^2. \tag{23}$$

In (22), (23), and for the rest of the paper, the subscript R stands for R_1 or R_2 for sake of generality because the links $\mathcal{S} \to \mathcal{R}_1 \to \mathcal{D}$ and $\mathcal{S} \to \mathcal{R}_2 \to \mathcal{D}$ can be treated in the same way. To derive the PEP, we differentiate three cases based on the relation of L_{RD} and L_{SR} because of the different characteristics of fading $\mathcal{S} \to \mathcal{R}$ and $\mathcal{R} \to \mathcal{D}$.

Case 1 ($L_{RD} > L_{SR}$). We consider (22) and define $Z_1 = d_1^2 = X_1Y_1$, where $X_1 = \sum_{l_{RD}=0}^{L_{RD}}|\mathbf{h}_{RD}(l_{RD})|^2$ and $Y_1 = \sum_{l_{SR}=0}^{L_{SR}}\boldsymbol{\lambda}(l_{SR})|\boldsymbol{\nu}(l_{SR})|^2$. Applying Chernoff bound, the PEP corresponding to d_1^2 is upper bounded by $E_{Z_1}[\exp(-\alpha^2Z_1/4N_0)] = \Phi_{Z_1}(s)|_{s=-\alpha^2/4N_0}$, where $\Phi(\cdot)$ denotes the moment-generating function. If we consider $\mathcal{R}_1$

($\mathcal{R}_2$), α will be corresponding to α_1 (α_2). $\Phi_{Z_1}(s)$ can be evaluated as [14]

$$\Phi_{Z_1}(s) = \int_0^\infty f_{X_1}(x_1)\Phi_{Y_1}(sx_1)dx_1, \tag{24}$$

where $f(\cdot)$ is the probability density function. Since the fading channels $\mathcal{S} \to \mathcal{R}$ and $\mathcal{R} \to \mathcal{D}$ are frequency-selective Rician and Rayleigh fading, respectively,

$$\Phi_{Y_1}(s) = \prod_{l_{SR}=0}^{L_{SR}} \left[\frac{1+n^2}{1+n^2-s\boldsymbol{\lambda}(l_{SR})} e^{[n^2 s\boldsymbol{\lambda}(l_{SR})/(1+n^2-s\boldsymbol{\lambda}(l_{SR}))]} \right], \tag{25}$$

$$f_{X_1}(x_1) = \frac{(L_{RD}+1)^{L_{RD}+1}}{\Gamma(L_{RD}+1)} x_1^{L_{RD}} e^{-(L_{RD}+1)x_1}, \tag{26}$$

where n is the Nakagami-n or Rician fading parameter, and $\Gamma(\cdot)$ represents the Gamma function defined by $\Gamma(k) \triangleq (k-1)!$ for any positive integer k.

Substituting (26) and (25) into (24), we have

$$\begin{aligned}\Phi_{Z_1}(s)\big|_{s=-\alpha^2/4N_0} &= \int_0^\infty \frac{(L_{RD}+1)^{L_{RD}+1}}{\Gamma(L_{RD}+1)} x_1^{L_{RD}} e^{-(L_{RD}+1)x_1} \\ &\quad \times \prod_{l_{SR}=0}^{L_{SR}} \left[\frac{1+n^2}{1+n^2+(\alpha^2/4N_0)x_1\boldsymbol{\lambda}(l_{SR})} \right. \\ &\quad \left. \times e^{-n^2(\alpha^2/4N_0)x_1\boldsymbol{\lambda}(l_{SR})/(1+n^2+(\alpha^2/4N_0)x_1\boldsymbol{\lambda}(l_{SR}))} \right] dx_1.\end{aligned} \tag{27}$$

We can rewrite (27) as

$$\begin{aligned}\Phi_{Z_1}(s)\big|_{s=-\alpha^2/4N_0} &= \frac{(L_{RD}+1)^{L_{RD}+1}}{\Gamma(L_{RD}+1)} \int_0^\infty x_1^{L_{RD}} e^{-(L_{RD}+1)x_1} \\ &\quad \times \prod_{l_{SR}=0}^{L_{SR}} \left[\frac{e^{-x_1/(x_1/n^2+((1+n^2)/n^2)/(\alpha^2/4N_0)\boldsymbol{\lambda}(l_{SR}))}}{(\alpha^2/4N_0)\boldsymbol{\lambda}(l_{SR})[x_1/(1+n^2)+1/(\alpha^2/4N_0)\boldsymbol{\lambda}(l_{SR})]} \right] dx_1,\end{aligned} \tag{28}$$

Assuming high signal-to-noise ratio (SNR), that is, $\alpha^2/4N_0 \gg 1$ and $(1+n^2)/n^2 \approx 1$, (28) can be evaluated as

$$\begin{aligned}\Phi_{Z_1}(s)\big|_{s=-\alpha^2/4N_0} &\approx \frac{(L_{RD}+1)^{L_{RD}+1}}{\Gamma(L_{RD}+1)} \left(\frac{\alpha^2}{4N_0}\right)^{-(L_{SR}+1)} \\ &\quad \times (1+n^2)^{L_{SR}+1} e^{-(L_{SR}+1)n^2} \prod_{l_{SR}=0}^{L_{SR}} \frac{1}{\boldsymbol{\lambda}(l_{SR})} \\ &\quad \times \int_0^\infty x_1^{L_{RD}-L_{SR}-1} e^{-(L_{RD}+1)x_1} dx_1.\end{aligned} \tag{29}$$

The integral in (29) when $L_{RD} > L_{SR}$ is given by [15]

$$\int_0^\infty x_1^{L_{RD}-L_{SR}-1} e^{-(L_{RD}+1)x_1} dx_1 = \frac{\Gamma(L_{RD}-L_{SR})}{(L_{RD}+1)^{L_{RD}-L_{SR}}}. \tag{30}$$

Substituting (30) into (29), we obtain

$$\begin{aligned}\Phi_{Z_1}(s)\big|_{s=-\alpha^2/4N_0} &\approx \left[\frac{(L_{RD}+1)(1+n^2)}{e^{n^2}} \right]^{L_{SR}+1} \\ &\quad \times \frac{\Gamma(L_{RD}-L_{SR})}{\Gamma(L_{RD}+1)} \left(\frac{\alpha^2}{4N_0}\right)^{-(L_{SR}+1)} \\ &\quad \times \prod_{l_{SR}=0}^{L_{SR}} \frac{1}{\boldsymbol{\lambda}(l_{SR})}.\end{aligned} \tag{31}$$

Case 2 ($L_{SR} > L_{RD}$). We examine (23) and similarly define $Z_2 = d_2^2 = X_2 Y_2$, where $X_2 = \sum_{l_{SR}=0}^{L_{SR}} |\mathbf{h}_{SR}(l_{SR})|^2$ and $Y_2 = \sum_{l_{RD}=0}^{L_{RD}} \boldsymbol{\lambda}(l_{RD})|\boldsymbol{\nu}(l_{RD})|^2$. Applying Chernoff bound, the PEP corresponding to d_2^2 is upper bounded by $E_{Z_2}[\exp(-\alpha^2 Z_2/4N_0)] = \Phi_{Z_2}(s)|_{s=-\alpha^2/4N_0}$ which is given by

$$\Phi_{Z_2}(s) = \int_0^\infty f_{X_2}(x_2)\Phi_{Y_2}(sx_2)dx_2, \tag{32}$$

where

$$\begin{aligned}f_{X_2}(x_2) &= \frac{(L_{SR}+1)^{1-L_{SR}/2}}{n^{L_{SR}}} \\ &\quad \times \frac{x_2^{L_{SR}/2} I_{L_{SR}}\left[2(L_{SR}+1)^{3/2} n x_2^{1/2}\right]}{e^{(L_{SR}+1)^2 n^2-(L_{SR}+1)x_2}},\end{aligned} \tag{33}$$

$$\Phi_{Y_2}(s) = \prod_{l_{RD}=0}^{L_{RD}} \frac{1}{1-s\boldsymbol{\lambda}(l_{RD})}. \tag{34}$$

The modified Bessel function of the first kind, $I_\alpha(\beta)$ in (33), is defined as

$$I_\alpha(\beta) \triangleq \left(\frac{1}{2}\beta\right)^\alpha \sum_{k=0}^\infty \frac{((1/4)\beta^2)^k}{k!\Gamma(\alpha+k+1)}, \quad \alpha \in \mathbb{R}. \tag{35}$$

Substituting (33) and (34) into (32), we have

$$\begin{aligned}\Phi_{Z_2}(s)\big|_{s=-\alpha^2/4N_0} &= \int_0^\infty \frac{(L_{SR}+1)^{1-L_{SR}/2} x_2^{L_{SR}/2}}{n^{L_{SR}} e^{(L_{SR}+1)^2 n^2-(L_{SR}+1)x_2}} \\ &\quad \times I_{L_{SR}}\left[2(L_{SR}+1)^{3/2} n x_2^{1/2}\right] \\ &\quad \times \prod_{l_{RD}=0}^{L_{RD}} \left[\frac{1}{1+(\alpha^2/4N_0)x_2\boldsymbol{\lambda}(l_{RD})} \right] dx_2.\end{aligned} \tag{36}$$

Under the assumption of high SNR ($\alpha^2/4N_0 \gg 1$), (36) can be computed as

$$\begin{aligned}\Phi_{Z_2}(s)\big|_{s=-\alpha^2/4N_0} &\approx \left(\frac{\alpha^2}{4N_0}\right)^{-(L_{RD}+1)} \frac{(L_{SR}+1)^{1-L_{SR}/2}}{n^{L_{SR}} e^{(L_{SR}+1)^2 n^2}} \prod_{l_{RD}=0}^{L_{RD}} \frac{1}{\boldsymbol{\lambda}(l_{RD})} \\ &\quad \times \int_0^\infty \frac{x_2^{L_{SR}/2-L_{RD}-1} I_{L_{SR}}\left[2(L_{SR}+1)^{3/2} n x_2^{1/2}\right]}{e^{(L_{SR}+1)x_2}} dx_2.\end{aligned} \tag{37}$$

Let $\xi \triangleq \int_0^\infty x_2^{L_{SR}/2-L_{RD}-1} e^{-(L_{SR}+1)x_2} I_{L_{SR}}[2(L_{SR}+1)^{3/2} n x_2^{1/2}]dx_2$. After some mathematical manipulations [15], we obtain

$$\begin{aligned}\xi &= (L_{SR}+1)^{L_{SR}/2+L_{RD}} n^{L_{SR}} \Gamma(L_{SR}-L_{RD}) \\ &\quad \times {}_1\widetilde{F}_1\left[L_{SR}-L_{RD}; L_{SR}+1; (L_{SR}+1)^2 n^2\right],\end{aligned} \tag{38}$$

where ${}_1\widetilde{F}_1(a;b;z)$ is hypergeometric ${}_1F_1$-regularized function and is defined as

$$\begin{aligned}{}_1\widetilde{F}_1(a;b;z) &\triangleq \frac{{}_1F_1(a;b;z)}{\Gamma(b)} \\ &= \frac{\sum_{k=0}^{\infty}\left(((a)_k/(b)_k)\left(z^k/k!\right)\right)}{\Gamma(b)}.\end{aligned} \tag{39}$$

Substituting (38) into (37), we obtain

$$\begin{aligned}\Phi_{Z_2}(s)\big|_{s=-\alpha^2/4N_0} &\approx \frac{(L_{SR}+1)^{L_{RD}+1}\Gamma(L_{SR}-L_{RD})}{e^{(L_{SR}+1)^2 n^2}} \\ &\quad \times {}_1\widetilde{F}_1\left(L_{SR}-L_{RD}; L_{SR}+1; (L_{SR}+1)^2 n^2\right) \\ &\quad \times \left(\frac{\alpha^2}{4N_0}\right)^{-(L_{RD}+1)} \prod_{l_{RD}=0}^{L_{RD}} \frac{1}{\boldsymbol{\lambda}(l_{RD})}.\end{aligned} \tag{40}$$

Case 3 ($L_{SR} = L_{RD}$). Considering (22), $\Phi_{Z_1}(s)$ can be calculated as

$$\begin{aligned}&\Phi_{Z_1}(s)\big|_{s=-\alpha^2/4N_0} \\ &= \frac{(L_{SR}+1)^{L_{SR}+1}}{\Gamma(L_{SR}+1)e^{(L_{SR}+1)n^2}} \left(\frac{\alpha^2}{4N_0}\right)^{-(L_{SR}+1)} \\ &\times \prod_{l_{SR}=0}^{L_{SR}} \left[\frac{1}{\boldsymbol{\lambda}(l_{SR})} \right. \\ &\qquad \left. \times \int_0^\infty \frac{x_1^{L_{SR}} e^{-(L_{SR}+1)x_1}}{\prod_{l_{SR}=0}^{L_{SR}}[(x_1/(1+n^2)) + 1/(\alpha^2/4N_0)\boldsymbol{\lambda}(l_{SR})]} dx_1\right].\end{aligned} \tag{41}$$

Let $t_1 = x_1/(1+n^2)$, (41) can be rewritten as

$$\begin{aligned}&\Phi_{Z_1}(s)\big|_{s=-\alpha^2/4N_0} \\ &= \frac{(L_{SR}+1)^{L_{SR}+1}(1+n^2)^{L_{SR}+1}}{\Gamma(L_{SR}+1)e^{(L_{SR}+1)n^2}} \left(\frac{\alpha^2}{4N_0}\right)^{-(L_{SR}+1)} \\ &\quad \times \prod_{l_{SR}=0}^{L_{SR}} \left[\frac{1}{\boldsymbol{\lambda}(l_{SR})} \int_0^\infty \frac{t_1^{L_{SR}} e^{-(L_{SR}+1)(1+n^2)t_1}}{\prod_{l_{SR}=0}^{L_{SR}}[t_1 + 1/(\alpha^2/4N_0)\boldsymbol{\lambda}(l_{SR})]} dt_1\right].\end{aligned} \tag{42}$$

Let us define

$$\zeta \triangleq \prod_{l_{SR}=0}^{L_{SR}} \left[\frac{1}{\boldsymbol{\lambda}(l_{SR})} \int_0^\infty \frac{t_1^{L_{SR}} e^{-(L_{SR}+1)(1+n^2)t_1}}{\prod_{l_{SR}=0}^{L_{SR}}[t_1 + 1/(\alpha^2/4N_0)\boldsymbol{\lambda}(l_{SR})]} dt_1\right]. \tag{43}$$

By using some mathematical expansions [15], we can express ζ as

$$\zeta = \sum_{l_{SR}=0}^{L_{SR}} \left[\left(\frac{\alpha^2}{4N_0}\right)^{L_{SR}} \frac{p_{l_{SR}}}{\boldsymbol{\lambda}(l_{SR})} \int_0^\infty \frac{t_1^{L_{SR}} e^{-(L_{SR}+1)(1+n^2)t_1}}{t_1 + 1/(\alpha^2/4N_0)\boldsymbol{\lambda}(l_{SR})} dt_1\right], \tag{44}$$

where $p_{l_{SR}} \triangleq \prod_{l=0, l\neq l_{SR}}^{L_{SR}} \boldsymbol{\lambda}(l_{SR})/[\boldsymbol{\lambda}(l_{SR}) - \boldsymbol{\lambda}(l)]$. Calculating the integral in (44), the value of ζ is evaluated as [15]

$$\begin{aligned}\zeta &= \sum_{l_{SR}=0}^{L_{SR}} \frac{p_{l_{SR}}}{[\boldsymbol{\lambda}(l_{SR})]^{L_{SR}+1}} e^{(L_{SR}+1)(n^2+1)/(\alpha^2/4N_0)\boldsymbol{\lambda}(l_{SR})} \\ &\quad \times \Gamma(L_{SR}+1)\Gamma\left[-L_{SR}, \frac{(L_{SR}+1)(n^2+1)}{(\alpha^2/4N_0)\boldsymbol{\lambda}(l_{SR})}\right],\end{aligned} \tag{45}$$

where the incomplete Gamma function is defined by $\Gamma[\alpha, x] \triangleq \int_x^\infty t^{\alpha-1}e^{-t}dt$.

Substituting ζ into (42), we have

$$\begin{aligned}&\Phi_{Z_1}(s)\big|_{s=-\alpha^2/4N_0} \\ &= \left[\frac{(L_{SR}+1)(1+n^2)}{e^{n^2}}\right]^{L_{SR}+1} \left(\frac{\alpha^2}{4N_0}\right)^{-(L_{SR}+1)} \\ &\quad \times \sum_{l_{SR}=0}^{L_{SR}} \left[\frac{p_{l_{SR}}}{[\boldsymbol{\lambda}(l_{SR})]^{L_{SR}+1}} e^{(L_{SR}+1)(n^2+1)/(\alpha^2/4N_0)\boldsymbol{\lambda}(l_{SR})} \right. \\ &\qquad \left. \times\Gamma\left[-L_{SR}, \frac{(L_{SR}+1)(n^2+1)}{(\alpha^2/4N_0)\boldsymbol{\lambda}(l_{SR})}\right]\right].\end{aligned} \tag{46}$$

Generalizing the three above cases with (31), (40) and (46), we can conclude that the diversity gain of our proposed DSTBC is $\min(L_{SR_1}, L_{R_1D}) + \min(L_{SR_2}, L_{R_2D}) + 2$ by extracting the exponential terms of $\alpha^2/4N_0$. Although the Rician fading parameter n does not produce any diversity gain, it acts as a coding gain, and thus can improve the PEP.

We provide here one example of PEP calculation for the case $L_{R_1D} > L_{SR_1}$ and $L_{R_2D} > L_{SR_2}$. Suppose that $E_{SR_2}/N_0 = E_{R_1D}/N_0 = E_{R_2D}/N_0 \gg 1$ and $E_{SR_1}/N_0 > E_{SR_2}/N_0$, the normalization factor in (9) can then be approximated as $\alpha_1^2 \approx \alpha_2^2 \approx E_{SR_2}$. From the result in (31), the PEP is upper bounded by

$$\begin{aligned}\text{PEP} &\leq \left(1+n^2\right)^{L_{SR_1}+L_{SR_2}+2} e^{-(L_{SR_1}+L_{SR_2}+2)n^2} \\ &\quad \times \left(L_{R_1D}+1\right)^{L_{SR_1}+1} \left(L_{R_2D}+1\right)^{L_{SR_2}+1} \\ &\quad \times \frac{\Gamma(L_{R_1D}-L_{SR_1})}{\Gamma(L_{R_1D}+1)} \frac{\Gamma(L_{R_2D}-L_{SR_2})}{\Gamma(L_{R_2D}+1)} \left(\frac{E_{SR_2}}{4N_0}\right)^{-(L_{SR_1}+L_{SR_2}+2)} \\ &\quad \times \prod_{l_{SR_1}=0}^{L_{SR_1}} \frac{1}{\boldsymbol{\lambda}(l_{SR_1})} \prod_{l_{SR_2}=0}^{L_{SR_2}} \frac{1}{\boldsymbol{\lambda}(l_{SR_2})}.\end{aligned} \tag{47}$$

We observe that the diversity order of this case is $L_{SR_1} + L_{SR_2} + 2 = \min(L_{SR_1}, L_{R_1D}) + \min(L_{SR_2}, L_{R_2D}) + 2$. Additionally, PEP reduces to zero when the Rician parameter n goes to infinity. That explains the positive effect of LOS component on the quality of received signals.

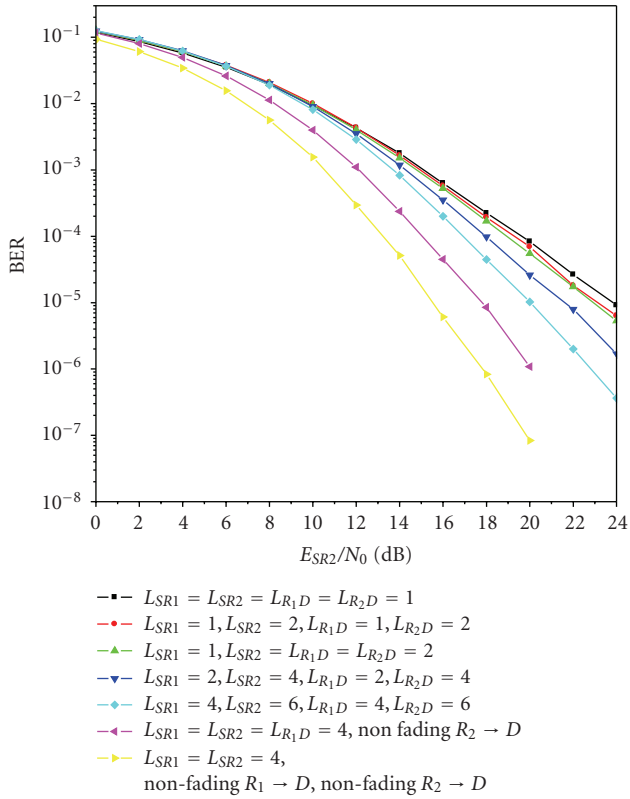

Figure 2: BER performance of DSTBC with FD-LE for various combinations of channel memory orders.

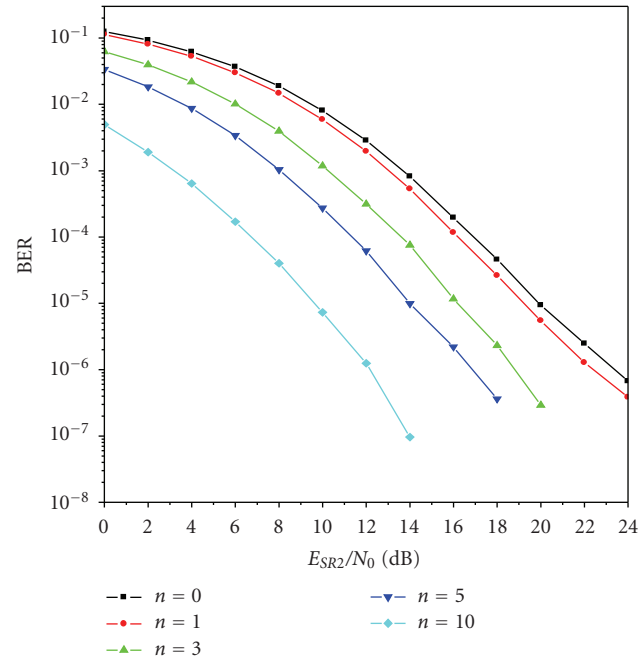

Figure 3: BER performance of DSTBC with different values of n-factor over Rician fading channels.

4. Numerical Results

As aforementioned, the PEP analysis is carried out based on (11). Moreover, the derivation of the PEP is accomplished under the assumption of an ML detection scheme at the receiver. However, such an ML scheme for the system model in our paper requires high complexity. Instead, we use MMSE frequency-domain linear equalizer to verify the analytical results. Since MMSE receiver is a suboptimal solution to the data detection problem, there is always a gap between the performance of ML and MMSE schemes. Note that the slopes of the performance curve of ML and MMSE receivers are similar at high SNR [16]. Consequently, the diversity gain can also be verified based on the performance of MMSE receiver.

In this section, we evaluate the BER performance of the proposed DSTBC via Monte Carlo simulation to justify the analysis of the achievable diversity gain. By observing the slope of these BER curves, we can confirm the validity of analysis since BER is proportional to PEP [16]. Each data block consists of 64 symbols including the zero sequence and information-carrying data which is modulated by QPSK with Gray mapping. We assume that the receiver has perfect channel state information.

Figure 2 shows the BER performances of the proposed DSTBC for various combinations of channel lengths using frequency domain linear equalizer (FD-LE), such as MMSE receiver. The fading $\mathcal{S} \to \mathcal{R}$ and $\mathcal{R} \to \mathcal{D}$ are assumed to be Rayleigh fading. We assume that the value of E_{SR_1}/N_0 is fixed at 25 dB, $E_{R_1D} = E_{R_2D} = 10$ dB, and plot the BER curves as a function of E_{SR_2}/N_0. Let us show the comparison of three cases.

Case 1. $L_{SR_1} = L_{SR_2} = L_{R_1D} = L_{R_2D} = 1$ (black curve and square marker); the diversity order is calculated by $\min(L_{SR_1}, L_{R_1D}) + \min(L_{SR_2}, L_{R_2D}) + 2 = L_{SR_1} + L_{SR_2} + 2 = 4$.

Case 2. $L_{SR_1} = 1$, $L_{SR_2} = 2$, $L_{R_1D} = 1$, $L_{R_2D} = 2$ (red curve and round marker); the diversity order is $L_{SR_1} + L_{SR_2} + 2 = 5$.

Case 3. $L_{SR_1} = 1$, $L_{SR_2} = L_{R_1D} = L_{R_2D} = 2$ (green curve and upper-triangular marker); the diversity order is $L_{SR_1} + L_{SR_2} + 2 = 5$.

The simulation results indicate that the slopes of the curves for Case 2 and Case 3 are steeper than that for Case 1 since Case 1 achieves smaller diversity gain. We can also see that the curves for Case 2 and Case 3 have the same slope, which can also be shown using the diversity order expressions we derived. These facts confirm our conclusion of the achievable diversity gain in the analysis. Another observation is for the same value of $L_{SR_1} = \min(L_{SR_1}, L_{R_1D}) = 1$ and $L_{SR_2} = \min(L_{SR_2}, L_{R_2D}) = 2$ (e.g., red curve and green curve), the better performance is achieved as the number of paths from the relays to destination increases. However the slopes of these BER curves are identical at high SNR since they have the same diversity gain of $L_{SR_1} + L_{SR_2} + 2 = 5$.

The performance of DSTBC over wireless fading channels where the fading $\mathcal{S} \to \mathcal{R}$ and $\mathcal{R} \to \mathcal{D}$ are characterized by Rician and Rayleigh distributions, respectively, is drawn in Figure 3 with different values of n-factor and the assumption

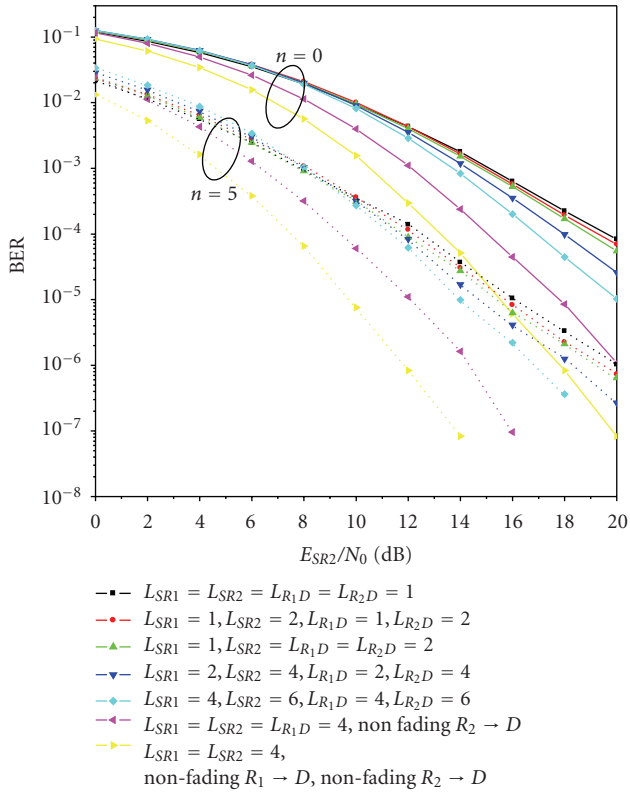

Figure 4: BER performance of DSTBC with different values of channel memory orders and n-factor over Rician fading channels.

of channel memory order of $L_{SR_1} = 4, L_{SR_2} = 6, L_{R_1D} = 4, L_{R_2D} = 6$. We remark that the better performance is achieved as the n-factor of Rician fading increases. However, the slopes of the performance curve are almost the same at high SNR, that is, they achieve the same diversity gain. This is because the term n only produces the coding gain to the PEP as we can see in the analysis. This confirms our conclusion about the achievable diversity gain from the PEP analysis mentioned in the previous section.

The performances of two cases $n = 0$ and $n = 5$ for various combinations of channel memory orders are shown in Figure 4 to study the effects of LOS component and channel memory orders on the BER. For each value of n, the BER curves corresponding to different channel memory orders are plotted to show the variations of slope due to different achievable diversity gains. We observe that the BER curves are shifted down if we increase n. That reflects the effect of LOS component on the coding gain through all range of SNR from low to high SNR. Meanwhile, the channel memory orders only have noticeable effects on the BER curves at high SNR caused by the change of diversity gain.

5. Conclusion

A DSTBC scheme for two-hop cooperative systems over frequency-selective fading channels has been proposed. The proposed DSTBC can achieve half-data rate transmission, spatial diversity order of $\min(L_{SR_1}, L_{R_1D}) + \min(L_{SR_2}, L_{R_2D}) + 2$. Furthermore, the data detection of the proposed DSTBC can be decoupled in frequency domain for a low-complexity receiver. The main idea in our design is that each relay conveys a distinct column of the conventional STBC developed for colocated antennas. We prove that the data rate of the proposed DSTBC is higher than that of repetition code which has the maximum data rate of 1/3 for a two-relay system. The design of DSTBC in our paper is inspired by the idea of linear dispersion codes where each column of the code matrix is a linear summation of transmit data and their conjugations [17]. In this paper, we analyze the PEP with a mixed Rayleigh and Rician frequency-selective fading channel model. The analysis shows that the LOS component effectively improves the error rate performance at the destination. Simulation results over different channel parameters and different n-factors were provided to verify the theoretical analysis.

Acknowledgments

This paper was partly supported by the IT R&D program of MKE/KEIT (KI001814, Game Theoretic Approach for Cross-layer Design in Wireless Communications) and MKE (The Ministry of Knowledge Economy), Korea, under the ITRC (Information Technology Research Center) support program supervised by the NIPA (National IT Industry Promotion Agency) (NIPA-2010-(C1090-1011-0001)).

References

[1] S. M. Alamouti, "A simple transmit diversity technique for wireless communications," *IEEE Journal on Selected Areas in Communications*, vol. 16, no. 8, pp. 1451–1458, 1998.

[2] V. Tarokh, H. Jafarkhani, and A. R. Calderbank, "Space-time block codes from orthogonal designs," *IEEE Transactions on Information Theory*, vol. 45, no. 5, pp. 1456–1467, 1999.

[3] A. Sendonaris, E. Erkip, and B. Aazhang, "User cooperation diversity—part I. System description," *IEEE Transactions on Communications*, vol. 51, no. 11, pp. 1927–1938, 2003.

[4] J. N. Laneman, D. N. C. Tse, and G. W. Wornell, "Cooperative diversity in wireless networks: efficient protocols and outage behavior," *IEEE Transactions on Information Theory*, vol. 50, no. 12, pp. 3062–3080, 2004.

[5] J. N. Laneman and G. W. Wornell, "Distributed space-time-coded protocols for exploiting cooperative diversity in wireless networks," *IEEE Transactions on Information Theory*, vol. 49, no. 10, pp. 2415–2425, 2003.

[6] Y. Jing and B. Hassibi, "Distributed space-time coding in wireless relay networks," *IEEE Transactions on Wireless Communications*, vol. 5, no. 12, pp. 3524–3536, 2006.

[7] Z. Yi and I.-M. Kim, "Single-symbol ML decodable distributed STBCs for cooperative networks," *IEEE Transactions on Information Theory*, vol. 53, no. 8, pp. 2977–2985, 2007.

[8] G. Scutari and S. Barbarossa, "Distributed space-time coding for regenerative relay networks," *IEEE Transactions on Wireless Communications*, vol. 4, no. 5, pp. 2387–2399, 2005.

[9] H. Mheidat, M. Uysal, and N. Al-Dhahir, "Equalization techniques for distributed space-time block codes with amplify-and-forward relaying," *IEEE Transactions on Signal Processing*, vol. 55, no. 5, pp. 1839–1852, 2007.

[10] S. Zhou and G. B. Giannakis, "Space-time coding with maximum diversity gains over frequency-selective fading channels," *IEEE Signal Processing Letters*, vol. 8, no. 10, pp. 269–272, 2001.

[11] N. Al-Dhahir, "Single-carrier frequency-domain equalization for space-time block-coded transmissions over frequency-selective fading channels," *IEEE Communications Letters*, vol. 5, no. 7, pp. 304–306, 2001.

[12] T. Wang and G. B. Giannakis, "Complex field network coding for multiuser cooperative communications," *IEEE Journal on Selected Areas in Communications*, vol. 26, no. 3, pp. 561–571, 2008.

[13] D. Falconer, S. L. Ariyavisitakul, A. Benyamin-Seeyar, and B. Eidson, "Frequency domain equalization for single-carrier broadband wireless systems," *IEEE Communications Magazine*, vol. 40, no. 4, pp. 58–66, 2002.

[14] A. Stuart and J. K. Ord, *Kendall's Advanced Theory of Statistics*, C. Griffin, London, UK, 5th edition, 1987.

[15] I. S. Gradshteyn and I. M. Ryzhik, *Table of Integrals, Series, and Products*, Academic Press, San Diego, Calif, USA, 7th edition, 2007.

[16] J. G. Proakis, *Digital Communications*, McGraw Hill, New York, NY, USA, 4th edition, 2001.

[17] B. Hassibi and B. M. Hochwald, "High-rate codes that are linear in space and time," *IEEE Transactions on Information Theory*, vol. 48, no. 7, pp. 1804–1824, 2002.